ADVANCED MATERIALS
www.advmat.de

Multitasking MXene Inks Enable High-Performance Printable Microelectrochemical Energy Storage Devices for All-Flexible Self-Powered Integrated Systems

Shuanghao Zheng, Hui Wang, Pratteek Das, Ying Zhang, Yuexian Cao, Jiaxin Ma, Shengzhong (Frank) Liu, and Zhong-Shuai Wu**

The future of mankind holds great promise for things like the Internet of Things, personal health monitoring systems, and smart cities. To achieve this ambitious goal, it is imperative for electronics to be wearable, environmentally sustainable, and safe. However, large-scale manufacture of self-sufficient electronic systems by exploiting multifunctional materials still faces significant hurdles. Herein, multitasking aqueous printable MXene inks are reported as an additive-free high-capacitance electrode, sensitive pressure-sensing material, highly conducting current collector, metal-free interconnector, and conductive binder. By directly screen printing MXene inks, MXene-based micro-supercapacitors (MSCs) and lithium-ion microbatteries (LIMBs) are delicately fabricated on various substrates. The as-prepared MSCs exhibit ultrahigh areal capacitance of 1.1 F cm^{-2} and the serially connected MSCs offer a record voltage of 60 V. The quasi-solid-state LIMBs deliver a robust areal energy density of 154 μWh cm^{-2}. Furthermore, an all-flexible self-powered integrated system on a single substrate based on the multitasking MXene inks is demonstrated through seamless integration of a tandem solar cell, the LIMB, and an MXene hydrogel pressure sensor. Notably, this integrated system is exceptionally sensitive to body movements with a fast response time of 35 ms. Therefore, this multipurpose MXene ink opens a new avenue for powering future smart appliances.

The growing trends in electronic devices like the Internet of Things, artificial intelligence, and healthcare monitoring have further stimulated the pursuit of miniaturized flexible electronics with sensitive functions, durability, extended lifetime, and great compatibility.[1–8] The full integration of miniaturized energy harvesters (e.g., solar cells, nanogenerators, thermoelectric devices), energy storage (e.g., supercapacitors and batteries), and energy consuming devices (e.g., sensors) into a self-powered integrated microsystem on a single substrate is widely considered a feasible route to fulfill the aforementioned requirements.[9–13] Such systems can convert light, vibration, or heat from the ambient environment into electrical energy that is instantly stored in the internal power source to be utilized anytime and anywhere.[14,15] For instance, graphene-based micro-supercapacitors (MSCs) can store electrical energy converted from sunlight by a solar cell and then power light-emitting diodes;[16] and polymer-based MSCs charged by a nanogenerator can stably drive pressure and gas sensors.[17] However, most of such integrated systems have been constructed by employing cumbersome fabrication methods (e.g., photolithography, laser cutting, evaporation, electrodeposition) while employing primitive assembling technologies are unable to guarantee good compatibility.[18–20] Printing techniques, such as screen printing, inkjet printing, and 3D printing, with beneficial features such as full additiveness, cost-effectiveness, high throughput, and environmental friendliness, have exhibited great potential for integrated circuits and targeted functional devices, such as for energy storage, gas detection, and health monitoring.[21–23] Among the printing techniques, screen

Dr. S. Zheng, P. Das, Y. Zhang, J. Ma, Prof. Z.-S. Wu
State Key Laboratory of Catalysis
Dalian Institute of Chemical Physics
Chinese Academy of Sciences
457 Zhongshan Road, Dalian 116023, China
E-mail: wuzs@dicp.ac.cn

Dr. S. Zheng, Prof. H. Wang, Dr. Y. Cao, Prof. S. (F.) Liu, Prof. Z.-S. Wu
Dalian National Laboratory for Clean Energy
Dalian Institute of Chemical Physics
Chinese Academy of Sciences
457 Zhongshan Road, Dalian 116023, China
E-mail: szliu@dicp.ac.cn

P. Das, Y. Zhang, J. Ma
University of Chinese Academy of Sciences
19 A Yuquan Rd, Shijingshan District, Beijing 100049, China

Prof. S. (F.) Liu
Key Laboratory of Applied Surface and Colloid Chemistry
Ministry of Education
Shaanxi Engineering Lab for Advanced Energy Technology
School of Materials Science and Engineering
Shaanxi Normal University
Xi'an 710119, China

The ORCID identification number(s) for the author(s) of this article can be found under https://doi.org/10.1002/adma.202005449.

DOI: 10.1002/adma.202005449

printing enables scaling with high throughput, as the roll-to-roll mode can be adopted, but the greater challenge lies in fabricating the multitasking ink.

MXenes, an emerging class of transition metal carbides, nitrides, and carbonitrides, have the general formula $M_{n+1}X_nT_x$ (n = 1, 2, or 3), where M represents the transition metal, X denotes carbon or nitrogen, and T is the multiple terminations (e.g., −F, −OH, −O).[24–26] In particular, $Ti_3C_2T_x$, the most widely studied MXene, has unique electrochemical, electrical, optical, and mechanical properties that endow it with great promise for use in applications like energy conversion, electronics, transparent films, electromagnetic interference shielding, and sensors.[24,27,28] Of particular interest to us, is its large energy storage capacity, metallic conductivity, and solution-processability that help in the creation of various printable microelectronic devices.[29–31] Using screen-printed MXene inks as active materials, MSCs have been exploited.[32–34] However, substantial additives or unexfoliated MXene sediment existed in the inks, leading to unsatisfactory electrical conductivity of the printed electrodes and low areal capacitance (<300 mF cm^{-2}). Moreover, MXene inks for full batteries with high voltage and improved performance have not yet been achieved. Meanwhile, the abundant functional surface terminations and excellent mechanical properties allow MXene to form a hierarchically viscoelastic skeleton with great exposure of sensing sites, endowing it with high sensitivity to pressure, resistance, gas pollutants, and chemical agents.[28,35–37] Fully considering these intriguing multiple functions of MXene, it is feasible to integrate a multitasking MXene into one monolithic module with preferable compatibility.

Herein, we report aqueous printable multitasking MXene inks applied as a highly capacitive electrode, a sensitive sensing material, a metal-free current collector, a conductive interconnector, and adhesive additives on a single substrate. Benefiting from the outstanding rheology of MXene capacitive inks and MXene-based battery-type inks, MXene-based MSCs (MX-MSCs) and lithium-ion microbatteries (MX-LIMBs) are constructed via screen printing in a versatile and scalable manner on various substrates, including A4 paper, wood, fabric, SiO_x-coated stainless steel, etc. Notably, the MX-MSCs delivered ultrahigh areal capacitance of 1.1 F cm^{-2} and energy density of 13.8 μWh cm^{-2}, both of which are much higher than most reported MX-MSCs. Impressively, a highly integrated MSCs pack consisting of 100 serially-connected MX-MSCs output a high voltage of 60 V, the highest value for MX-MSCs so far. Furthermore, the quasi-solid-state MX-LIMBs, composed of only active materials and MXene, presented an increased areal energy density of 154 μWh cm^{-2}. Taking full advantage of multitasking MXene inks, an all-flexible MXene-based self-powered integrated system, composed of a tandem thin-film silicon solar cell (Si-SC), a MX-LIMB, and a MXene hydrogel pressure sensor on a flexible co-planar substrate is demonstrated that sensitively monitors the bending of body parts with a fast response of 35 ms.

The procedures for screen-printing aqueous MXene-based inks for the stepwise fabrication of MX-MSCs, MX-LIMBs, and the all-flexible MXene-based self-powered integrated system are schematically presented in **Figure 1**. Pure aqueous MXene ink was directly printed on the substrate through the screen mesh with specific patterns (e.g., interdigitated shape) to fabricate MX-MSCs (Figure 1a). The well-designed screen-printing process allows precise deposition of ink at high throughput. For the construction of MX-LIMBs, aqueous MXene-based lithium titanate (LTO) and lithium iron phosphate (LFP) inks were printed step-by-step on each side of the aforementioned MXene-based current collectors (Figure 1b). As a proof-of-concept for multitasking MXene inks in electronics, the self-powered integrated system was achieved by first depositing

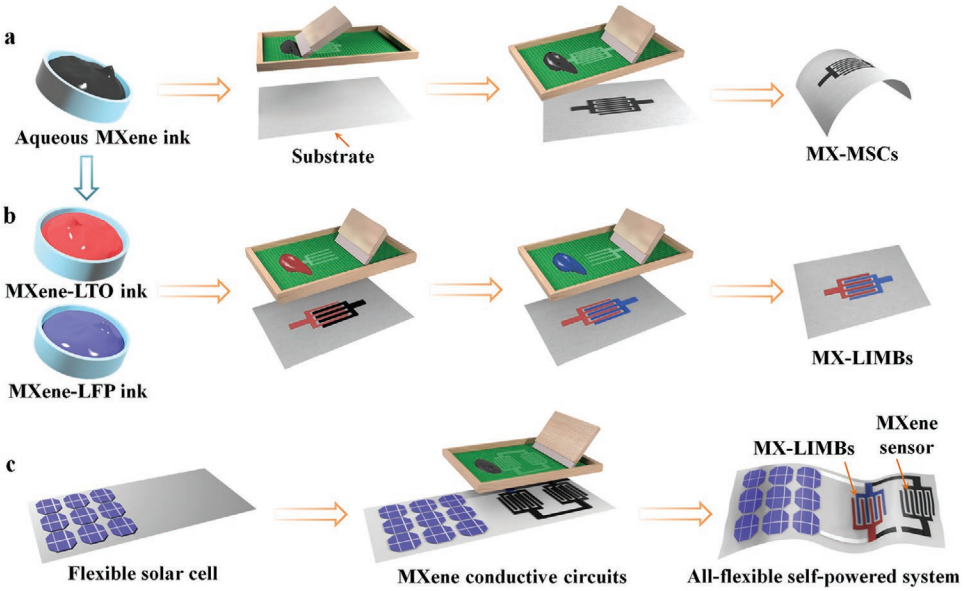

Figure 1. Schematic of the fabrication of printable MX-MSCs, MX-LIMBs, and all-flexible self-powered integrated system. a) Schematic illustration of MX-MSCs from direct screen printing of aqueous MXene ink. b) Schematic fabrication of MX-LIMBs from stepwise screen printing of aqueous MXene-based LTO and LFP inks. c) Schematic construction of the self-powered sensor system by step-by-step screen printing of MX-LIMBs and an MXene hydrogel sensor with the PECVD grown Si-SC on the same side of one flexible substrate.

a tandem Si-SC on a flexible stainless-steel substrate via plasma enhanced chemical vapor deposition (PECVD). It should be emphasized that, to electrically isolate the solar cell from the other components, the substrate was coated with an insulating SiO_x layer. On this layer, MXene-based current collectors and interconnectors were printed for the subsequent precise deposition of the MX-LIMBs and MXene hydrogel pressure sensor in their respective places to complete the fabrication process (Figure 1c). It is noted that this is the first prototype demonstration of such an all-flexible, self-powered, integrated system with a co-planar geometry constructed on a single substrate.

To examine the suitability for screen printing, two kinds of MXene inks with different concentrations were synthesized from the selective etching of Ti_3AlC_2 in a mixture of LiF/HCl (**Figure 2**a,b). The MXene nanosheets in the aqueous inks exhibited a 2D delaminated structure (Figure 2c), large interlayer spacing of 1.2 nm (Figure S1a, Supporting Information), lateral size of up to 10 µm (Figure S1b, Supporting Information), and ultrathin thickness of 2.1 nm with most nanosheets being less than three layers (Figure S2, Supporting Information). One of the inks was the highly concentrated MXene ink (denoted as H-MXene ink, Figure 2a) with the mass ratio of ≈10 wt% (≈100 mg mL^{-1}, ≈3.4 vol%), while the other was the less-concentrated MXene ink (L-MXene ink, Figure 2b) with a concentration of ≈2 wt% (≈20 mg mL^{-1}, ≈0.7 vol%). During tube inversion tests, the H-MXene ink displayed obviously higher viscosity than the L-MXene ink making it the prime candidate for the subsequent printing process. To confirm this, the rheological properties of the H-MXene and L-MXene inks were measured. Importantly, both of them presented a typical shear-thinning behavior with increasing shear rate (Figure 2d), indicating the behavior of non-Newtonian fluids. This rheological behavior essentially enables the continuous extrusion of the MXene ink during the screen-printing process. Remarkably, the H-MXene ink at the shear rate of 0.05 s^{-1} delivered a much higher apparent viscosity of 3548 Pa·s than the L-MXene ink (26 Pa·s), suggestive of the better extrusion of the H-MXene ink. By utilizing alternating low (0.1 s^{-1}) and high (100 s^{-1}) shear rates, a sudden reduction of apparent viscosity was found at the high shear rate, and an instantaneous recovery was discovered

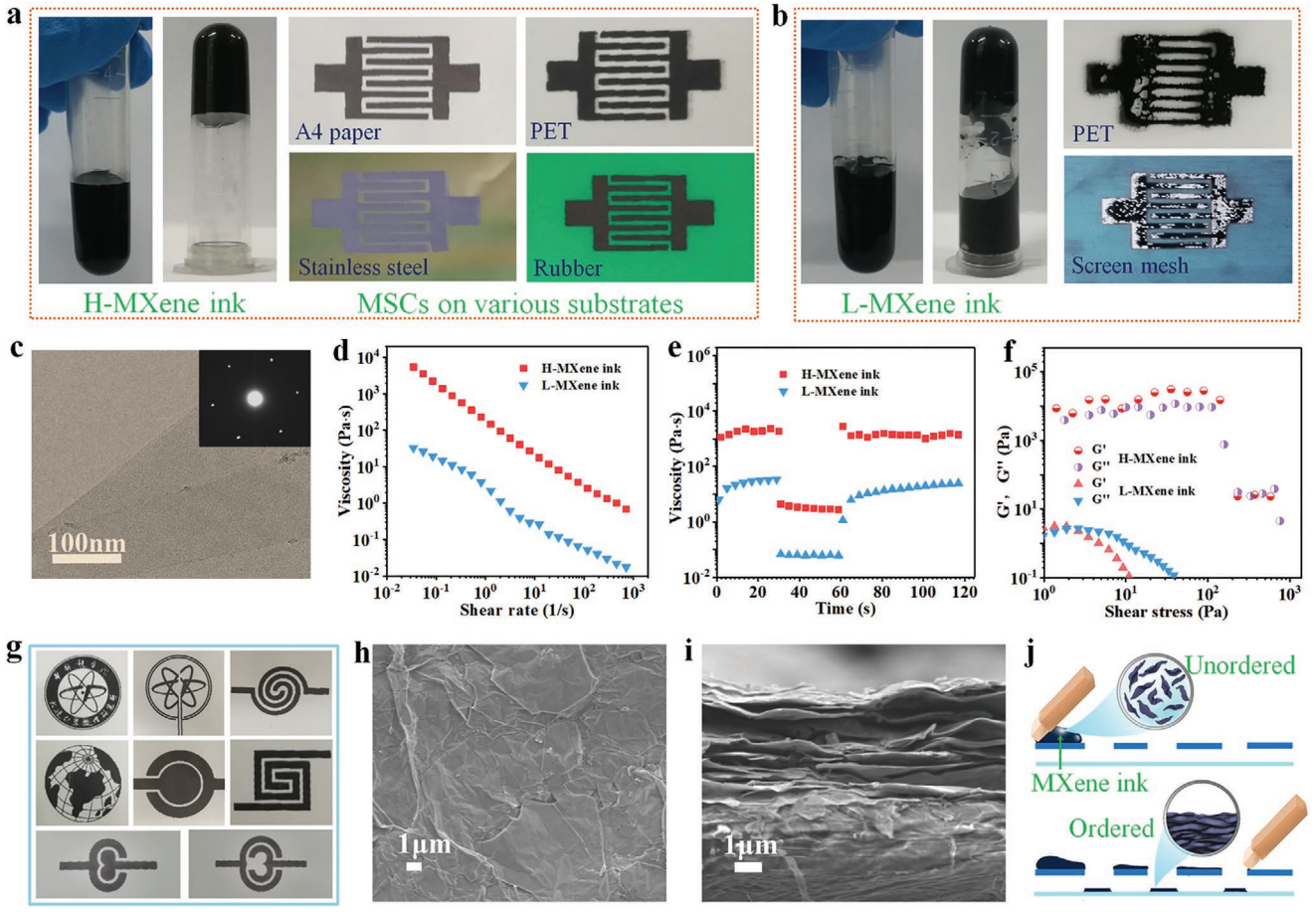

Figure 2. Properties and characterization of aqueous MXene inks. a) Optical images of aqueous H-MXene ink in the normal and inverted states (left) and the fabricated MX-MSCs on various substrates (right). b) Optical images of L-MXene ink in the normal and inverted states (left), the prepared MX-MSCs on PET substrate and the used screen mesh after screen printing (right). c) Transmission electron microscopy and selected-area electron diffraction images of MXene nanosheets. d) Apparent viscosity of H-MXene and L-MXene inks versus shear rate. e) Viscosity evolution of H-MXene and L-MXene inks as a function of the alternating low (0.1 s^{-1}) and high (100 s^{-1}) shear rates. f) Storage modulus and loss modulus of H-MXene and L-MXene inks versus shear stress. g) Photographs of various screen-printed MXene patterns, including the "DICP" logo, the earth and MX-MSCs with different shapes. h) Top-view and i) cross-sectional SEM images of the screen-printed MXene films. j) Schematic illustration of the orderly aligned MXene nanosheets after the shear interaction.

when the shear rate recovered (Figure 2e). Such highly elastic rheological property of MXene inks is essential to maintain the architectures of the printed patterns and prevent them from short-circuiting. The viscosity of L-MXene ink increased over time at low shear rate, indicative of the unstable structure and liquid-like fluidity. Furthermore, the H-MXene ink exhibited both a high storage modulus (G') and a high loss modulus (G'') with a solid-like behavior until the shear stress reached the yield stress of ≈200 Pa (Figure 2f). When the stress surpassed the yield point, the G' and G'' of the H-MXene ink declined abruptly, indicating its liquid-like behavior in the high shear stress region. The high yield stress of the H-MXene ink was favorable for the continuous extrusion and immediate solidification of the printed MXene.

As expected, the H-MXene ink could be smoothly extruded from the screen mesh onto various substrates (right of Figure 2a and Figure S3, Supporting Information), such as A4 paper, polyethylene terephthalate (PET), SiO_x-coated stainless steel, rubber, glass, wood, and non-woven fabric. Unsurprisingly, the printed shapes of the L-MXene ink were ambiguous and short-circuited, and even the screen mesh was blocked by the printed L-MXene ink (right of Figure 2b and Figure S4, Supporting Information). This happened due to the low elastic modulus and small yield stress (3 Pa, Figure 2f), likely resulting from excessive water solvent. The printed MXene films adapted remarkably to flexible and stretchable substrates (Figures S5 and S6, Supporting Information). The H-MXene ink showed a low zeta potential of −43.8 mV (Figure S7, Supporting Information), which was primarily responsible for the stability and homogeneity of this ink. Therefore, an additive-free aqueous MXene ink for screen printing was achieved. Because of factors like suitable viscosity, high elasticity, and robust viscosity recovery, aqueous MXene ink could be directly and precisely printed on the A4 paper with both simple and intricate patterns (Figure 2g), for example, "DICP" logo, the earth and other shapes, demonstrative of shape diversity and wide applicability. The designed configurations were able to be precisely stacked by repeated printing. Scanning electron microscopy (SEM) images of the printed MXene microelectrodes showed a flat, continuous and intact structure of MXene nanosheets (Figure 2h), forming a highly conductive network (≈500 S cm^{-1}). It was observed that MXene nanosheets in the microelectrodes were parallelly aligned (Figure 2i), resulting from the shear flow interaction during the printing process (Figure 2j). This orderly stacked lamellar architecture of MXene microelectrodes is very beneficial to ion transfer along the plane of the MXene nanosheet.[38,39]

To evaluate the electrochemical performance, the as-printed MX-MSCs with the interdigitated pattern on A4 paper were tested with H_2SO_4/polyvinyl alcohol (PVA) gel electrolyte. As seen in **Figure 3**a, MX-MSCs showed typical quasi-rectangular CV curves, indicative of outstanding capacitive behavior. To increase the areal capacitance, MX-MSCs printed with 1, 5, and 10 printed layers were constructed and denoted as MX-MSCs-1L, MX-MSCs-5L, and MX-MSCs-10L, respectively. With increasing number of printed layers, the charge and discharge time at 0.4 mA cm^{-2} were extensively increased (Figure 3b), suggesting enhanced capacitance. MX-MSCs-10L (Figure 3c) with an electrode thickness of ≈20 µm displayed higher areal capacitance of 1108 mF cm^{-2} in comparison with MX-MSCs-5L (615 mF cm^{-2}) and MX-MSCs-1L (44 mF cm^{-2}). The low areal capacitance and rate capability of MX-MSCs-1L resulted from an incomplete electrically conductive network of the discontinuous MXene film on the A4 paper with rough surface (inset of Figure 3d), leading to the small slope of the I–V curve (1.5 mA V^{-1}, Figure 3d), and high equivalent series resistance (103 Ω, Figure S8, Supporting Information). These traits are inferior to those of MX-MSCs-5L (18 mA V^{-1}, 15 Ω) and MX-MSCs-10L (26 mA V^{-1}, 9 Ω). It is worth noting that the high areal capacitance (1108 mF cm^{-2}) outperforms all previously reported MSCs fabricated by screen printing (Table S1, Supporting Information), and is comparable to the 3D-printed MSCs with thick electrodes of hundreds of micrometers (0.5–3 F cm^{-2})[40–43] or 3D thick electrode structure (0.3–5 F cm^{-2}).[44–47] Moreover, this value exceeds most reported MSCs (Figure 3e), such as graphene with metal oxides or polymers (400–300 mF cm^{-2}),[16,48] MXene hybrids (350–150 mF cm^{-2}),[34,49,50] and reduced graphene oxide (50–1 mF cm^{-2}),[51–53] Notably, MX-MSCs-5L revealed extraordinary cycling performance without capacitance fade after 10 000 cycles (Figure 3f). Additionally, MX-MSCs with different numbers of printed layers on varying substrates delivered considerable areal capacitance (Figures S9–S14, Supporting Information), for example, MX-MSCs-2L on glass (188 mF cm^{-2}), MX-MSCs-1L on PET (63 mF cm^{-2}), MX-MSCs-3L on wood (363 mF cm^{-2}), MX-MSCs-4L on non-woven fabric (218 mF cm^{-2}), MX-MSCs-1L on rubber (72 mF cm^{-2}), and MX-MSCs-2L on SiO_x-coated stainless steel (220 mF cm^{-2}), demonstrative of the wide applicability of this strategy. MX-MSCs on A4 paper, wood, and SiO_x-coated stainless steel delivered considerably high normalized areal capacitance (Figure S15, Supporting Information), which was primarily attributed to the abundant capillary channels or preferable wettability of these substrates. As a result, these substrates showed a higher mass loading of MXene with 0.8 to 0.95 mg cm^{-2} for each printing (Figure S16, Supporting Information). In other words, flat substrates with strong adsorption and wettability for printing ink are beneficial to better loading of ink and electrode structure with superb accessibility to electrolyte ions, eventually accounting for high electrochemical performance.

A Ragone plot was created to compare the MX-MSCs with the state-of-the-art reported MSCs. As shown in Figure 3g, MX-MSCs-10L presented a robust areal energy density of 13.8 µWh cm^{-2}, which was higher than the reported values (Tables S1 and S2, Supporting Information), for example, of HF-etched MXene MSCs (0.67 µWh cm^{-2}),[54] all-MXene MSCs (1.43 µWh cm^{-2}),[55] freeze- and thaw-assisted MXene MSCs (1.18 µWh cm^{-2}),[56] and graphene/MXene MSCs (0.85 µWh cm^{-2}).[57] Moreover, MX-MSCs-10L offered a high power density of 2.5 mW cm^{-2} with a considerable energy density of 6.4 µWh cm^{-2}. In addition, MX-MSCs on A4 paper showed outstanding flexibility, as indicated by the overlapped CV curves measured at various degrees of bending from the flat state to 180° (Figure 3h), showing the great potential for flexible and wearable microelectronics.

In order to meet the demand of microelectronic devices (e.g., microrobots, microsensors), integrated MSCs connected in series and/or parallel are essential to output tailored voltage and

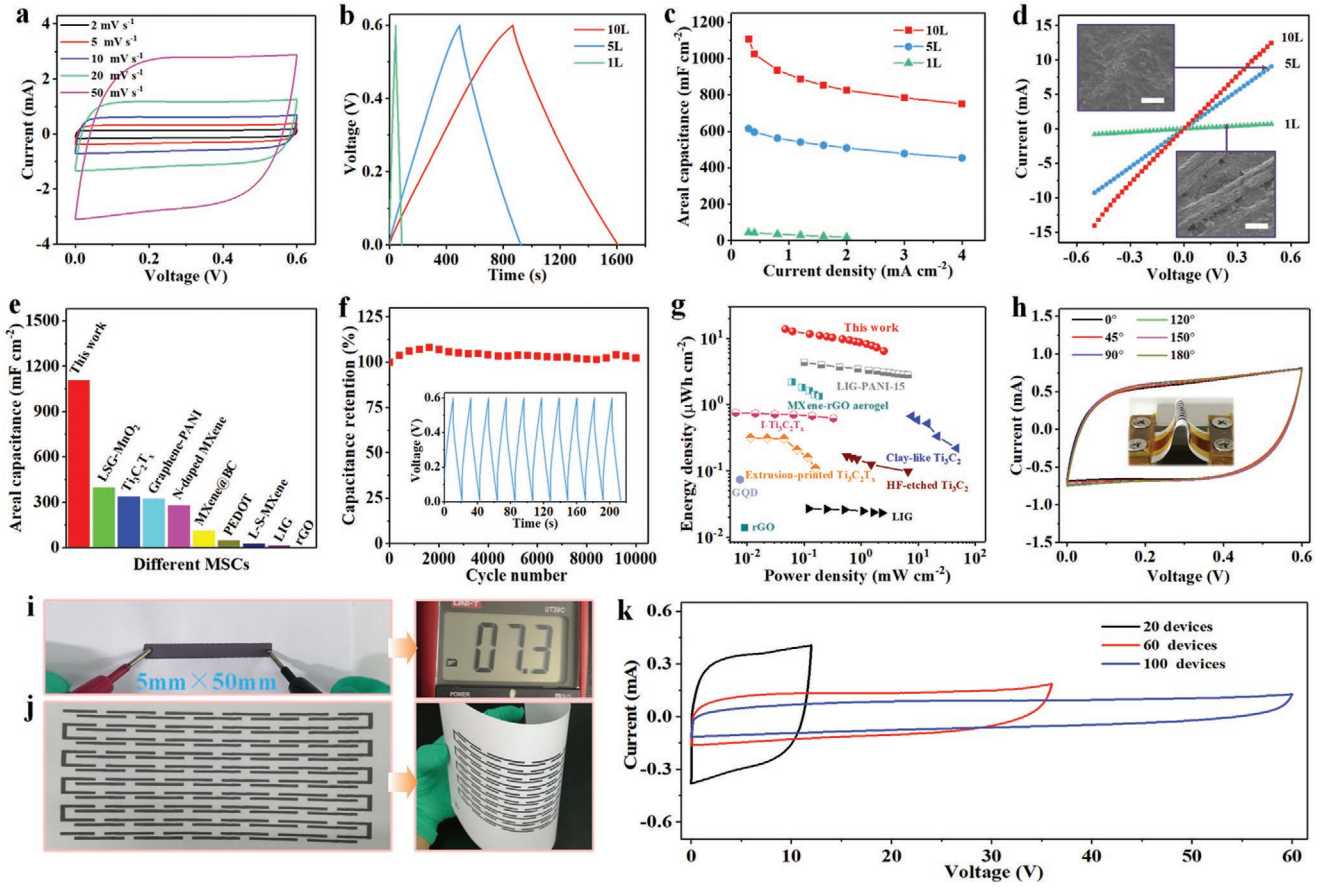

Figure 3. Electrochemical performance of MX-MSCs printed on A4 paper. a) CV curves measured from 2 to 50 mV s^{-1}. b) GCD profiles obtained at 0.4 mA cm^{-2} and c) areal capacitance of MX-MSCs-1L, MX-MSCs-5L, and MX-MSCs-10L. d) *I–V* curves of MXene film with 1, 5, and 10 printed layers. The insets are SEM images of MXene film on A4 paper with a scale bar of 10 μm. e) Comparison of areal capacitance of this work to those of other reported MSCs. f) Cycling stability obtained at 3 mA cm^{-2}. Inset is the last ten cycles of GCD profiles. g) Ragone plot of MX-MSCs compared with the reported MSCs based on MXene and graphene. h) CV curves tested at various bending states at 100 mV s^{-1}. Inset is the bending state of 180°. i) Resistance of the printed MXene film. j) Photographs of 100 tandem linear MX-MSCs in the flat and bent states. k) CV curves of 20, 60, and 100 tandem MX-MSCs.

current. It was revealed that the metal-free MXene connections with low resistance (7.3 Ω, Figure 3i) were comparable to the commercial carbon-coated Al foil (1.3 Ω, Figure S17, Supporting Information). By combining the exceptional MXene ink, highly conducting MXene and versatile printing process, integrated MX-MSCs with aesthetic features could be readily realized in only one step, such as the serially-connected MX-MSCs with the geometries of linear shapes (Figure 3j), parallel strips (inset of Figure S18a, Supporting Information), and interdigitated patterns (inset of Figure S19a, Supporting Information). It is of special note that the tandem MX-MSCs used only MXene as highly capacitive microelectrodes and conducting connections free of additives, binders, metal current collectors, and interconnects. The serially-connected MX-MSCs with parallel strips and interdigitated pattern showed linearly enlarged voltage and unchanged discharge time with increasing number of individual cells (Figures S18 and S19, Supporting Information), indicating the extraordinary performance uniformity. Remarkably, 100 tandem MX-MSCs were rapidly fabricated in one second. Such modular MX-MSCs pack output an ultrahigh voltage of 60 V (Figure 3k), suggestive of the great opportunity for modular integrated circuits.

To demonstrate the multifunctionality of MXene as a versatile platform for depositing active battery materials, aqueous MXene-based LTO and LFP inks were further prepared by uniformly hybridizing conducting MXene ink (30 wt%) with LTO or LFP (70 wt%), respectively (**Figure 4**a). The resulting MXene-based LTO and LFP inks exhibited a prominent shear-thinning phenomenon, showing the viscosities of 3428 and 6923 Pa·s at 0.05 s^{-1} (Figure 4b), respectively. For fabricating MX-LIMBs (left of Figure 4a), a MXene-based current collector was initially printed on A4 paper using aqueous MXene ink, followed by accurate deposition of the patterned MXene-based LTO anode and LFP cathode on each side of the MXene-based current collectors. The printed MXene-based LTO and LFP microelectrodes, with characteristic diffraction peaks of both MXene and LTO or LFP (Figure 4c), revealed almost no separated interface between the current collectors and the microelectrodes (Figure 4d–f). Moreover, these microelectrodes exhibited a uniform structure (Figure 4e–h and Figure S20, Supporting Information), in which LTO and LFP particles were entirely embedded into the conducting MXene nanosheet skeleton, enabling rather low sheet resistances of 8 and 6 Ω $\square^{-1}$ (Figure S21, Supporting Information), corresponding to

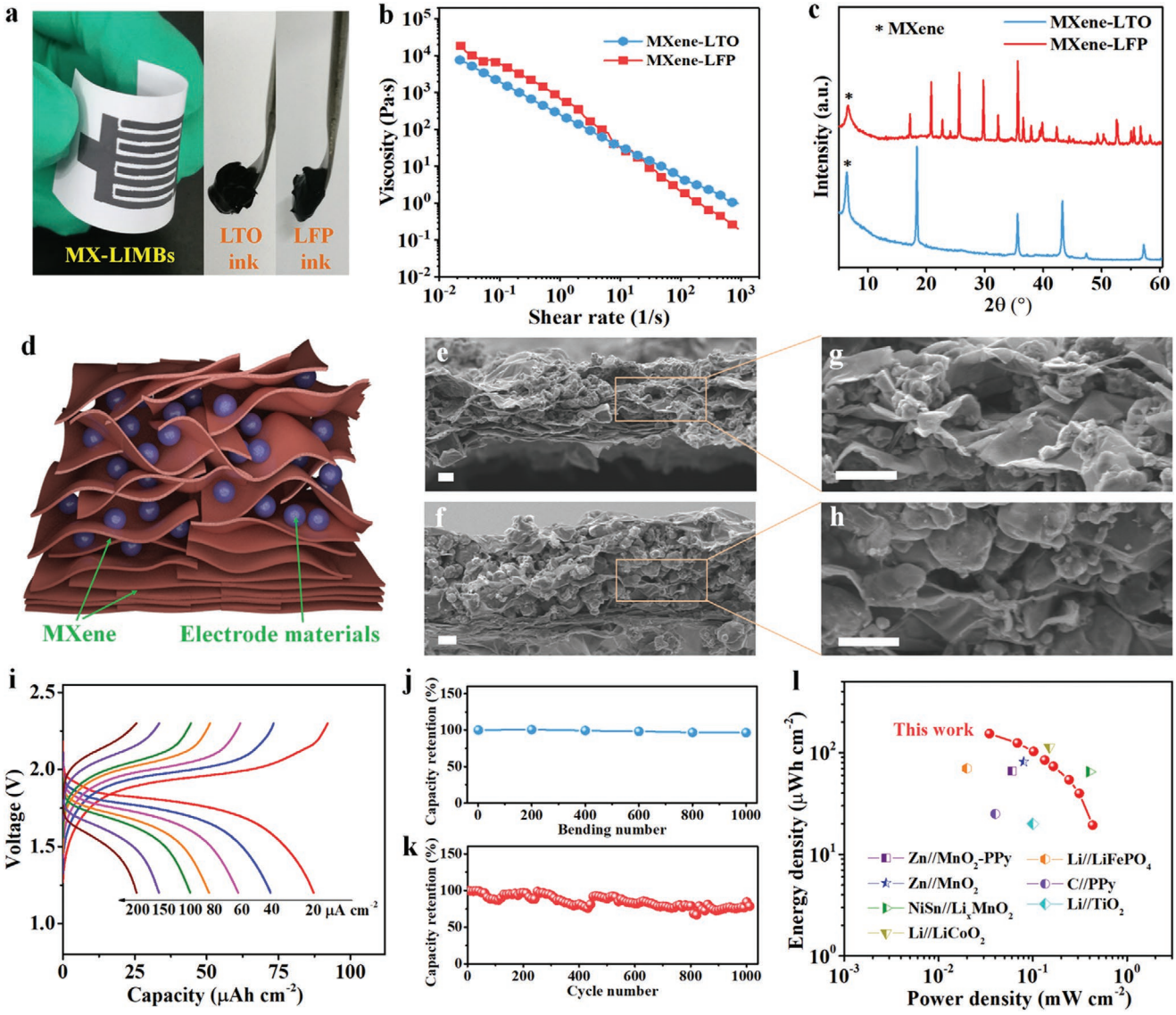

Figure 4. Characterization of aqueous MXene-based LTO and LFP inks and electrochemical performance of MX-LIMBs. a) Optical images of MXene-based LTO and LFP inks and the fabricated MX-LIMBs. b) Apparent viscosity of MXene-based LTO and LFP inks. c) XRD patterns of MXene-based LTO and LFP microelectrodes. d) Schematic structure of the printed microelectrodes. e–h) Cross-sectional SEM images of the printed MXene-based LTO (e,g) and LFP (f,h) microelectrodes. The scale bars in (e–h) are 1 μm. i) GCD profiles measured at varying current densities, j) capacity retention under repeated bending, and k) cycle performance of MX-LIMBs. l) Ragone plot of MX-LIMBs to compare with the previous MBs.

electrical conductivities of 42 and 55 S cm^{-1}, respectively. Note that the whole printing process was free of the commonly used binder polymers, conducting additives, and organic solvents, indicating the environmentally friendly benefits of the entire microbattery fabrication process. It is worth emphasizing that this is the first time such aqueous battery-type MXene inks have been achieved for LIMBs.

The fabricated MX-LIMBs operating in an ionogel electrolyte ($LiTFSI/P_{14}TFSI$/PVDF-HFP, made up of bis(trifluoromethanesulfonyl)imide lithium salt, 1-butyl-1-methylpyrrolidinium, bis(trifluoromethyl-sulfonyl)imide, and poly(vinylidene-difluoride-*co*-hexafluoropropylene)), displayed a couple of redox peaks at 2.0 and 1.7 V (Figure S22, Supporting Information), revealing a battery-like feature. Furthermore, the MX-LIMBs, with a stable discharge plateau at 1.75 V, delivered high areal discharge capacity of 88 μAh cm^{-2} at a current density of 20 μA cm^{-2} (Figure 4d), and a better rate capability with areal capacity of 46 μAh cm^{-2} at 100 μA cm^{-2} was achieved (Figure S23, Supporting Information). Notably, MX-LIMBs presented excellent flexibility without capacity loss even after repeated bending for 1000 cycles (Figure 4j), ascribed to the highly flexible scaffold formed by the MXene. Moreover, the MX-LIMBs delivered acceptable cyclability with a capacity retention of 82% after 1000 cycles (Figure 4k). Remarkably, the areal energy density of the MX-LIMBs reached 154 μWh cm^{-2} (Figure 4l), which is one order of magnitude higher than that of the MX-MSCs (13.8 μWh cm^{-2}), and superior to those of most reported MBs, such as $Li//LiCoO_2$ (113 μWh cm^{-2}),[58]

NiSn//Li_xMnO_2 (65 μWh cm^{-2}),[59] Zn//MnO_2 (81.5 μWh cm^{-2}),[60] Zn//MnO_2-polypyrrole (PPy) (66 μWh cm^{-2}),[61] and Li//$LiFeO_4$ (70 μWh cm^{-2}).[62]

To demonstrate the unprecedented potential role of multitasking MXene in smart devices, an all-flexible self-powered integrated system of MX-LIMBs (or MX-MSCs) and a MXene hydrogel sensor was fabricated through a continuous screen printing process to seamlessly couple with a tandem Si-SC on the flexible stainless steel substrate (thickness of 30 μm) (**Figures 5**a,b and 1c; Figure S24, Supporting Information). To construct the pressure sensor, PVA and MXene ink were mixed with the crosslinking agent, borax, to form MXene-based hydrogel as a pressure sensing material (Figure S25, Supporting Information). By virtue of its sticky nature, the MXene-based hydrogel adhered easily to both the MXene-based current collector and the substrate. Impressively, the MX-MSCs as a microscale energy storage device could power the pressure sensor (Figure S26, Supporting Information), but they suffered from a considerably fast self-discharge rate (1 h from 1.2 to 0.7 V) (Figure S27, Supporting Information). Although the self-discharge rate of MXene-based supercapacitors was efficiently reduced by chemically interface-tailored regulation,[63] further improvement is still highly required. To extend the durability of operation, new MX-LIMBs were constructed, presenting a longer self-discharge time from 2.3 to 1.8 V over 9 h (Figure 5c). Ultimately, the all-flexible self-powered integrated system contained a tandem Si-SC as the energy harvester, MX-LIMBs for energy storage, and a MXene hydrogel pressure sensor for signal detection (Figure 5a,b), capable of operating independently without any external charging circuit.

Notably, in this all-flexible self-powered integrated system, MXene was fully utilized as the high-performance active material

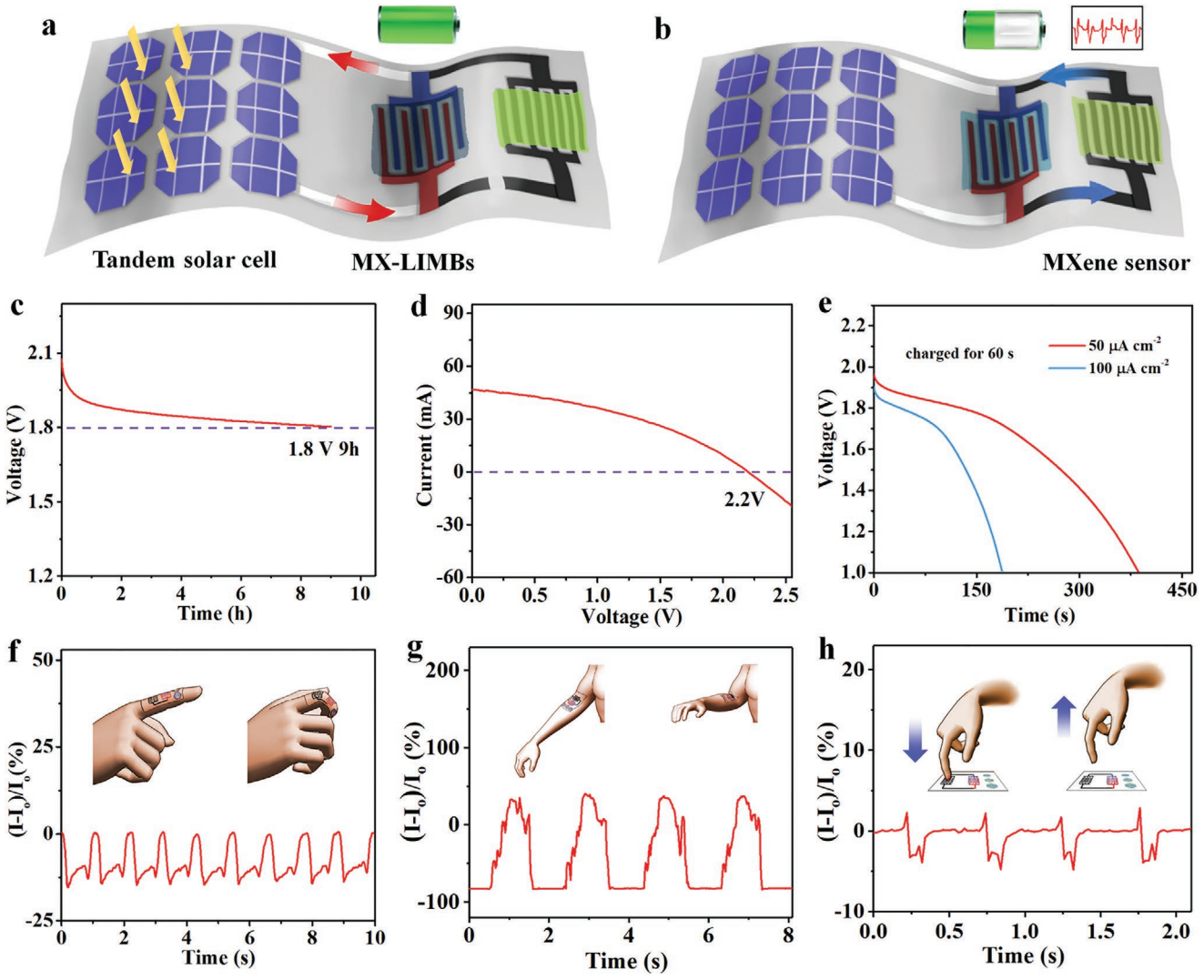

Figure 5. All-flexible MXene-based self-powered integrated system for pressure sensing. a) Schematic of the process for charging by the flexible tandem Si-SC. b) Schematic of the process with the sensor powered by the MX-LIMB. c) Self-discharge profile of the MX-LIMB. d) *I–V* curve of the flexible tandem Si-SC on the stainless-steel substrate. e) Discharge curves of the MX-LIMB at different current densities after charging by the tandem Si-SC for 60 s. f–h) Current change of the MXene hydrogel sensor powered by the integrated MX-LIMBs in response to the bending of a finger (f), the bending of an elbow (g), and pressing vertically (h).

electrode, pressure-sensing material, current collector, metal-free interconnects, and conductive binder, without the involvement of the commonly used organic solvents and polymer binders, demonstrative of the great potential of multitasking MXene inks. Three tandem Si-SCs with the size of 8 cm×6 cm exhibited a higher output voltage of 2.2 V (Figure 5d). Once charged by the tandem Si-SCs for 60 s, the MX-LIMB was capable of galvanostatically discharging for 390 and 180 s at 50 and 100 μA cm^{-2}, respectively (Figure 5e). Meanwhile, the MX-LIMB outputs a stable voltage for the efficient utilization of the pressure sensor to monitor bodily motions via an electromechanical response. Initially, the MXene-based hydrogel sensor was attached to the outside of a finger joint. When the finger was bent repeatedly, a clear and stable current waveform with ≈12% variation of the initial current was generated (Figure 5f), due to the tensile deformation of the MXene hydrogel. Afterward, when the MXene hydrogel sensor was adhered to the elbow, an anisotropic response (current increase and decrease) was recorded (Figure 5g), ascribed to the compressive and tensile strains during the deformation. Moreover, the MXene hydrogel sensor could be employed as a pressure-sensing film to quickly register the touch motion with an ultralow response time of only 35 ms (Figure 5h and Figure S28, Supporting Information), reflecting the remarkable sensitivity of this self-powered integrated system. These exceptional results indicated that the all-flexible MXene-based self-powered integrated system could serve as a standalone working unit to achieve the pressure-sensing function, demonstrating its tremendous opportunities for use in future smart wearable systems.

In summary, we have demonstrated printable multitasking MXene inks for highly compatible construction of MXene-based microscale energy storage devices and an all-flexible self-powered integrated system on a single flexible substrate. In this system, MXene acts as a highly capacitive electrode, sensitive sensing material, current collector, conducting interconnect, and adhesive additive, justifying its role as a multifunctional material. The developed aqueous additive-free MXene ink and MXene-based battery-type inks allowed for fast and scalable fabrication of MX-MSCs and MX-LIMBs with customized shapes on arbitrary insulating substrates. The as-prepared MX-MSCs exhibited ultrahigh areal capacitance (1.1 F cm^{-2}), outstanding flexibility, and high voltage output in series (60 V) while the MX-LIMBs offered exceptionally robust areal energy density (154 μWh cm^{-2}). Moreover, the as-assembled self-powered integrated system without the addition of an external power source was capable of sensitively and repeatedly monitoring deformation with a highly rapid response of only 35 ms. We believe that through further exploitation of new MXene-based materials with varying functional components, printable multitasking MXene inks will open a new avenue for scalable fabrication to realize the different yet highly integrated functions in one single device or system with broad applications in energy storage, optoelectronics, electronics, and sensing.

Experimental Section

Preparation of Aqueous MXene Ink: $Ti_3C_2T_x$ MXene was prepared by selectively etching Ti_3AlC_2 via LiF and HCl.[64,65] Typically, 2 g LiF (Kermel) was mixed with 9 M HCl (40 mL, Kermel), followed by slowly adding 1 g Ti_3AlC_2 (<40 μm, Y-Carbon, Ltd.). Then, the mixture was etched at 35 °C for 24 h with stirring. After etching, the mixture was centrifuged (5000 rpm, 5 min) and washed four times with deionized water. Later, 20 mL water was added to the collected $Ti_3C_2T_x$ sediment and fast vibration was carried out for 20 min. Afterward, the obtained $Ti_3C_2T_x$ dispersion was centrifuged at 2000 rpm for 5 min to discard the non-etched Ti_3AlC_2 or unexfoliated $Ti_3C_2T_x$ and then subsequently centrifuged at 5000 rpm for 5 min to collect the fully exfoliated $Ti_3C_2T_x$ MXene. Finally, pure aqueous $Ti_3C_2T_x$ MXene ink with a desirable concentration, for example, ≈100 mg mL^{-1} for screen printing, was achieved.

Preparation of MXene-Based LTO and LFP Inks: 0.23 g LTO (from FDK) or LTP (from BTR) powder was uniformly mixed with H-MXene ink (1 g) and a little water (50 μL) using ball-milling method under an inner atmosphere, in which the mass ratio of LTO or LTP and MXene was fixed at ≈7:3. To avoid the oxidation of MXene, the freshly prepared aqueous MXene-based LTO or LFP ink could be immediately printed through screen printing.

Fabrication of MX-MSCs: First, a screen mesh was fixed onto the printed substrate. Second, aqueous MXene ink was loaded onto the screen mesh and then swiftly screen printed onto the substrate. The screen (100–300 mesh) was made of polyester fabrics and had a coating layer of photosensitive adhesive (PLUS8000). The blade was made of polyurethane rubber with shore hardness of 85. When the blade was applied to fabricate the devices, the pressure of ≈0.4 MPa was used. After drying under vacuum at room temperature for 24 h and coating with aqueous H_2SO_4/PVA gel electrolyte and package, MX-MSCs were obtained. By repeated screen printing, a new MXene layer was precisely stacked on the former one after the former MXene layer was completely dried.

Fabrication of MX-LIMBs: MXene-based current collectors with two stacked MXene layers were initially printed on the A4 paper substrate using H-MXene ink. Then aqueous MXene-based LTO ink was deposited on one side of the MXene-based current collectors through the corresponding screen mesh to pattern the LTO anode for repeating four times. Subsequently, aqueous MXene-based LFP ink was precisely established on the other side of MXene-based current collectors to form LFP cathode micropatterns for repeating four times. After drying and coating with an ionogel electrolyte of LiTFSI-P_{14}TFSI-PVDF-HFP, the MX-LIMBs were achieved. The fabricated devices were carefully packaged with PDMS tested in ambient condition. For the preparation of the ionogel electrolyte, LiTFSI was initially added into P_{14}TFSI solvent to obtain 1 M LiTFSI-P_{14}TFSI. Next, PVDF-HFP (0.2 g) was dissolved into acetone under continuous stirring to form a transparent dispersion. Then, LiTFSI-P_{14}TFSI solution (2.5 g) was uniformly mixed with the PVDF-HFP dispersion under stirring. Finally, the ionogel electrolyte was prepared.

Fabrication of MXene-Based Sensor: 1 mL MXene ink (20 mg mL^{-1}) was slowly mixed into 10 mL aqueous PVA (100 mg mL^{-1}, Mw = 67 000, Aladdin) solution and the resulting mixture was continuously stirred for 1 h. Then the cross-linking agent borax (25 mg, Kermel) was added into the above dispersion to form the MXene-based hydrogel as the pressure-sensing material. Finally, the as-synthesized MXene-based hydrogel was carefully coated onto the interdigitated MXene-based current collector to obtain the MXene hydrogel sensor.

Assembly of the Self-Powered Integrated System: The all-flexible self-powered integrated system was constructed by a combined PECVD and screen printing process. A tandem Si-SC as the energy harvester was initially formed on the flexible stainless steel substrate via PECVD, and MX-LIMBs for energy storage and a MXene hydrogel pressure sensor for energy utilization were developed via screen printing. For the preparation of the tandem Si-SC, stainless steel with the thickness of 30 μm was uniformly coated with a silver layer (300 nm) by evaporation, followed by the deposition of a ZnO layer (100 nm) by sputtering. Next, an amorphous thin-film Si-SC with the size of 8 cm × 6 cm was constructed with the structure of P-doped Si(n)/Si(i)/B-doped Si(p) on the above modified substrate, followed by a repeat of the nip Si deposition to form three tandem Si-SCs with a high voltage output. After indium tin oxide was deposited on the top cell by E-beam evaporation and grids were laminated onto the ITO for current conduction, the tandem Si-SC was complete for integration with the MX-LIMB.

With regard to the integrated MX-LIMBs and MXene hydrogel pressure sensor, a thin SiO_x insulating layer was uniformly deposited onto the remaining unused space of the flexible stainless-steel substrate for the construction of the MXene-based LIMBs and sensor to avoid short circuits. Later, the patterned MXene-based current collectors and interconnectors were built using aqueous MXene ink on the SiO_x insulating layer of the flexible stainless steel substrate. Then aqueous MXene-based LTO ink was carefully printed on one side of the MXene-based current collector to form the LTO anode microelectrode, followed by the precise establishment of the MXene-based LFP cathode microelectrode via aqueous MXene-based LFP ink, and ionogel electrolyte was coated onto the LTO and LFP finger microelectrodes. Afterward, MXene-based hydrogel was accurately overlaid on the MXene-based current collector to establish the MXene-based sensor for pressure detection. After the encapsulation of the flexible substrate and prepared microdevices by a thin PDMS layer, the all-flexible MXene-based self-powered integrated system with a co-planar geometry on a single flexible substrate was completed.

Supporting Information

Supporting Information is available from the Wiley Online Library or from the author.

Acknowledgements

This work was financially supported by the National Key R@D Program of China (Grants 2016YBF0100100 and 2016YFA0200200), the National Natural Science Foundation of China (Grant Nos. 51872283, 22075279, 21805273, 51622210, 51872277, 22005297, 22005298), the Strategic Priority Research Program of Chinese Academy of Sciences (Grant No. XDA17040506), Dalian National Laboratory For Clean Energy (DNL), CAS, DNL Cooperation Fund, CAS (DNL180310, DNL180308, DNL201912, and DNL201915), the Liao Ning Revitalization Talents Program (Grant XLYC1807153), the Natural Science Foundation of Liaoning Province, Joint Research Fund Liaoning-Shenyang National Laboratory for Materials Science (Grant 20180510038), DICP (DICP ZZBS201708, DICP ZZBS201802, DICP I2020032), and DICP&QIBEBT (Grant DICP&QIBEBT UN201702), China Postdoctoral Science Foundation (Grant 2019M661141).

Conflict of Interest

The authors declare no conflict of interest.

Keywords

microbatteries, micro-supercapacitors, MXene inks, screen printing, self-powered integrated systems

Received: August 11, 2020
Revised: October 26, 2020
Published online: February 1, 2021

[1] W. Gao, S. Emaminejad, H. Y. Y. Nyein, S. Challa, K. Chen, A. Peck, H. M. Fahad, H. Ota, H. Shiraki, D. Kiriya, D.-H. Lien, G. A. Brooks, R. W. Davis, A. Javey, *Nature* **2016**, *529*, 509.
[2] Z. Y. Lin, Y. Huang, X. F. Duan, *Nat. Electron.* **2019**, *2*, 378.
[3] Y. Son, B. Frost, Y. Zhao, R. L. Peterson, *Nat. Electron.* **2019**, *2*, 540.
[4] B. D. Gates, *Science* **2009**, *323*, 1566.
[5] Y. Yang, W. Gao, *Chem. Soc. Rev.* **2019**, *48*, 1465.
[6] M. Bariya, H. Y. Y. Nyein, A. Javey, *Nat. Electron.* **2018**, *1*, 160.
[7] S. Niu, N. Matsuhisa, L. Beker, J. Li, S. Wang, J. Wang, Y. Jiang, X. Yan, Y. Yun, W. Burnett, A. S. Y. Poon, J. B. H. Tok, X. Chen, Z. Bao, *Nat. Electron.* **2019**, *2*, 361.
[8] T. R. Ray, J. Choi, A. J. Bandodkar, S. Krishnan, P. Gutruf, L. Tian, R. Ghaffari, J. A. Rogers, *Chem. Rev.* **2019**, *119*, 5461.
[9] K. Myny, *Nat. Electron.* **2018**, *1*, 30.
[10] S. Xu, Y. Qin, C. Xu, Y. Wei, R. Yang, Z. L. Wang, *Nat. Nanotechnol.* **2010**, *5*, 366.
[11] Z. Wen, M.-H. Yeh, H. Guo, J. Wang, Y. Zi, W. Xu, J. Deng, L. Zhu, X. Wang, C. Hu, L. Zhu, X. Sun, Z. L. Wang, *Sci. Adv.* **2016**, *2*, e1600097.
[12] J. Xu, Y. Chen, L. Dai, *Nat. Commun.* **2015**, *6*, 8103.
[13] J. Chen, Z. L. Wang, *Joule* **2017**, *1*, 480.
[14] P. Zhang, F. Wang, M. Yu, X. Zhuang, X. Feng, *Chem. Soc. Rev.* **2018**, *47*, 7426.
[15] S. Zheng, X. Shi, P. Das, Z.-S. Wu, X. Bao, *Adv. Mater.* **2019**, *31*, 1900583.
[16] M. F. El-Kady, M. Ihns, M. Li, J. Y. Hwang, M. F. Mousavi, L. Chaney, A. T. Lech, R. B. Kaner, *Proc. Natl. Acad. Sci. USA* **2015**, *112*, 4233.
[17] J. Ye, H. Tan, S. Wu, K. Ni, F. Pan, J. Liu, Z. Tao, Y. Qu, H. Ji, P. Simon, Y. Zhu, *Adv. Mater.* **2018**, *30*, 1801384.
[18] Y. Lu, K. Jiang, D. Chen, G. Z. Shen, *Nano Energy* **2019**, *58*, 624.
[19] J. Yun, C. Song, H. Lee, H. Park, Y. R. Jeong, J. W. Kim, S. W. Jin, S. Y. Oh, L. Sun, G. Zi, J. S. Ha, *Nano Energy* **2018**, *49*, 644.
[20] R. You, Y.-Q. Liu, Y.-L. Hao, D.-D. Han, Y.-L. Zhang, Z. You, *Adv. Mater.* **2020**, *32*, 1901981.
[21] Y.-Z. Zhang, Y. Wang, T. Cheng, L.-Q. Yao, X. Li, W.-Y. Lai, W. Huang, *Chem. Soc. Rev.* **2019**, *48*, 3229.
[22] J. T. Muth, D. M. Vogt, R. L. Truby, Y. Menguc, D. B. Kolesky, R. J. Wood, J. A. Lewis, *Adv. Mater.* **2014**, *26*, 6307.
[23] Y. Lin, J. Chen, M. M. Tavakoli, Y. Gao, Y. Zhu, D. Zhang, M. Kam, Z. He, Z. Fan, *Adv. Mater.* **2018**, *31*, 1804285.
[24] F. Shahzad, M. Alhabeb, C. B. Hatter, B. Anasori, S. Man Hong, C. M. Koo, Y. Gogotsi, *Science* **2016**, *353*, 1137.
[25] B. Anasori, M. R. Lukatskaya, Y. Gogotsi, *Nat. Rev. Mater.* **2017**, *2*, 16098.
[26] M. Ghidiu, M. R. Lukatskaya, M.-Q. Zhao, Y. Gogotsi, M. W. Barsoum, *Nature* **2014**, *516*, 78.
[27] Y. Gogotsi, B. Anasori, *ACS Nano* **2019**, *13*, 8491.
[28] Y. Ma, N. Liu, L. Li, X. Hu, Z. Zou, J. Wang, S. Luo, Y. Gao, *Nat. Commun.* **2017**, *8*, 1207.
[29] M. R. Lukatskaya, S. Kota, Z. Lin, M.-Q. Zhao, N. Shpigel, M. D. Levi, J. Halim, P.-L. Taberna, M. W. Barsoum, P. Simon, Y. Gogotsi, *Nat. Energy* **2017**, *6*, 17105.
[30] C. Zhang, S.-H. Park, A. Seral-Ascaso, S. Barwich, N. McEvoy, C. S. Boland, J. N. Coleman, Y. Gogotsi, V. Nicolosi, *Nat. Commun.* **2019**, *10*, 849.
[31] Y.-Z. Zhang, Y. Wang, Q. Jiang, J. K. El-Demellawi, H. Kim, H. N. Alshareef, *Adv. Mater.* **2020**, *32*, 1908486.
[32] H. Li, X. Li, J. Liang, Y. Chen, *Adv. Energy Mater.* **2019**, *9*, 1803987.
[33] S. Abdolhosseinzadeh, R. Schneider, A. Verma, J. Heier, F. Nüesch, C. Zhang, *Adv. Mater.* **2020**, *32*, 2000716.
[34] L. H. Yu, Z. D. Fan, Y. L. Shao, Z. N. Tian, J. Y. Sun, Z. F. Liu, *Adv. Energy Mater.* **2019**, *9*, 1901839.
[35] B. Xiao, Y.-c. Li, X.-f. Yu, J.-b. Cheng, *Sens. Actuators, B* **2016**, *235*, 103.
[36] Y. Cai, J. Shen, G. Ge, Y. Zhang, W. Jin, W. Huang, J. Shao, J. Yang, X. Dong, *ACS Nano* **2018**, *12*, 56.
[37] S. J. Kim, H.-J. Koh, C. E. Ren, O. Kwon, K. Maleski, S.-Y. Cho, B. Anasori, C.-K. Kim, Y.-K. Choi, J. Kim, Y. Gogotsi, H.-T. Jung, *ACS Nano* **2018**, *12*, 986.
[38] J. J. Yoo, K. Balakrishnan, J. Huang, V. Meunier, B. G. Sumpter, A. Srivastava, M. Conway, A. L. Mohana Reddy, J. Yu, R. Vajtai, P. M. Ajayan, *Nano Lett.* **2011**, *11*, 1423.

[39] Z. S. Wu, K. Parvez, X. L. Feng, K. Mullen, *Nat. Commun.* **2013**, *4*, 2487.
[40] B. Yao, S. Chandrasekaran, H. Zhang, A. Ma, J. Kang, L. Zhang, X. Lu, F. Qian, C. Zhu, E. B. Duoss, C. M. Spadaccini, M. A. Worsley, Y. Li, *Adv. Mater.* **2020**, *32*, 1906652.
[41] B. Yao, S. Chandrasekaran, J. Zhang, W. Xiao, F. Qian, C. Zhu, E. B. Duoss, C. M. Spadaccini, M. A. Worsley, Y. Li, *Joule* **2019**, *3*, 459.
[42] W. J. Yang, J. Yang, J. J. Byun, F. P. Moissinac, J. Q. Xu, S. J. Haigh, M. Domingos, M. A. Bissett, R. A. W. Dryfe, S. Barg, *Adv. Mater.* **2019**, *31*, 1902725.
[43] J. Orangi, F. Hamade, V. A. Davis, M. Beidaghi, *ACS Nano* **2020**, *14*, 640.
[44] T. Zhai, F. Wang, M. Yu, S. Xie, C. Liang, C. Li, F. Xiao, R. Tang, Q. Wu, X. Lu, Y. Tong, *Nanoscale* **2013**, *5*, 6790.
[45] Y. Song, T. Liu, B. Yao, M. Li, T. Kou, Z.-H. Huang, D.-Y. Feng, F. Wang, Y. Tong, X.-X. Liu, Y. Li, *ACS Energy Lett.* **2017**, *2*, 1752.
[46] D. Feng, T. Lei, M. R. Lukatskaya, J. Park, Z. Huang, M. Lee, L. Shaw, S. Chen, A. A. Yakovenko, A. Kulkarni, J. Xiao, K. Fredrickson, J. B. Tok, X. Zou, Y. Cui, Z. Bao, *Nat. Energy* **2018**, *3*, 30.
[47] D. S. Ashby, R. H. DeBlock, C.-H. Lai, C. S. Choi, B. S. Dunn, *Joule* **2017**, *1*, 344.
[48] Z. S. Wu, K. Parvez, S. Li, S. Yang, Z. Y. Liu, S. H. Liu, X. L. Feng, K. Müllen, *Adv. Mater.* **2015**, *27*, 4054.
[49] H. Huang, H. Su, H. Zhang, L. Xu, X. Chu, C. Hu, H. Liu, N. Chen, F. Liu, W. Deng, B. Gu, H. Zhang, W. Yang, *Adv. Electron. Mater.* **2018**, *4*, 1800179.
[50] Q. Jiang, Y. Lei, H. Liang, K. Xi, C. Xia, H. N. Alshareef, *Energy Storage Mater.* **2020**, *27*, 78.
[51] J. Lin, Z. Peng, Y. Liu, F. Ruiz-Zepeda, R. Ye, E. L. G. Samuel, M. J. Yacaman, B. I. Yakobson, J. M. Tour, *Nat. Commun.* **2014**, *5*, 5714.
[52] B. Xie, Y. Wang, W. Lai, W. Lin, Z. Lin, Z. Zhang, P. Zou, Y. Xu, S. Zhou, C. Yang, F. Kang, C.-P. Wong, *Nano Energy* **2016**, *26*, 276.
[53] Z.-S. Wu, Y.-Z. Tan, S. Zheng, S. Wang, K. Parvez, J. Qin, X. Shi, C. Sun, X. Bao, X. Feng, K. Müllen, *J. Am. Chem. Soc.* **2017**, *139*, 4506.
[54] N. Kurra, B. Ahmed, Y. Gogotsi, H. N. Alshareef, *Adv. Energy Mater.* **2016**, *6*, 1601372.
[55] Y.-Y. Peng, B. Akuzum, N. Kurra, M.-Q. Zhao, M. Alhabeb, B. Anasori, E. C. Kumbur, H. N. Alshareef, M.-D. Ger, Y. Gogotsi, *Energy Environ. Sci.* **2016**, *9*, 2847.
[56] X. Huang, P. Wu, *Adv. Funct. Mater.* **2020**, *30*, 1910048.
[57] H. Li, Y. Hou, F. Wang, M. R. Lohe, X. Zhuang, L. Niu, X. Feng, *Adv. Energy Mater.* **2017**, *7*, 1601847.
[58] S. W. Song, K. C. Lee, H. Y. Park, *J. Power Sources* **2016**, *328*, 311.
[59] H. L. Ning, J. H. Pikul, R. Y. Zhang, X. J. Li, S. Xu, J. J. Wang, J. A. Rogers, W. P. King, P. V. Braun, *Proc. Natl. Acad. Sci. USA* **2015**, *112*, 6573.
[60] G. Q. Sun, X. T. Jin, H. S. Yang, J. Gao, L. T. Qu, *J. Mater. Chem. A* **2018**, *6*, 10926.
[61] M. Zhu, Z. Wang, H. Li, Y. Xiong, Z. Liu, Z. Tang, Y. Huang, A. L. Rogach, C. Zhi, *Energy Environ. Sci.* **2018**, *11*, 2414.
[62] H. Lee, S. Kim, K.-B. Kim, J.-W. Choi, *Nano Energy* **2018**, *53*, 225.
[63] Z. Wang, Z. Xu, H. Huang, X. Chu, Y. Xie, D. Xiong, C. Yan, H. Zhao, H. Zhang, W. Yang, *ACS Nano* **2020**, *14*, 4916.
[64] Y. Xia, T. S. Mathis, M.-Q. Zhao, B. Anasori, A. Dang, Z. Zhou, H. Cho, Y. Gogotsi, S. Yang, *Nature* **2018**, *557*, 409.
[65] M. Alhabeb, K. Maleski, B. Anasori, P. Lelyukh, L. Clark, S. Sin, Y. Gogotsi, *Chem. Mater.* **2017**, *29*, 7633.